2008 10th Intl. Conf. on Control, Automation, Robotics and Vision
Hanoi, Vietnam, 17–20 December 2008

Design and Simulation of Wireless, Walking Scratch-Drive Micro-Robot

Eakkasit Dumsong[†§], Nitin Afzulpurkar[†¤], *Member*, *IEEE*, Adisorn Tuantranont[‡¡] and Chumnarn Punyasai[*¢]
[†] School of Engineering and Technology, Asian Institute of Technology, P.O. Box 4, Klong Luang, Pathumthani 12120, Thailand
[‡] Nanoelectronics and MEMS laboratory, National Electronics and Computer Technology Center, Klongluang, Pathumtani 12120, Thailand
[*] Thailand IC Design and Innovation Laboratory, National Electronics and Computer Technology Center, Klongluang, Pathumtani 12120, Thailand
Email: [§] Eakkasit.Dumsong@ait.ac.th, [¤] nitin@ait.ac.th, [¡] adisorn.tuantranont@nectec.or.th, [¢] chumnarn.punyasai@nectec.or.th

***Abstract*—We present the design of prototype electrostatic scratch-drive micro-robot with dimensions of 365 µm x75 µm. The micro-robot consists of three scratch drive actuators (SDA) and two steering arms. The method of motion is controlled by delivering power via capacitive coupling, with an underlying electric grid, to micro-robot. Then, micro-robot can move freely without connected wire. The behavior of micro-robot using analytical solutions and FEM simulation (ANSYS) has been investigated.**

***Keywords*— micro-robot, scratch drive actuators, wireless, capacitive coupling**

I. INTRODUCTION

In 1959, Professor Richard Feynman addressed the potential of manipulating and controlling things on small scale in famous lecture "There's plenty of room at the bottom". The solution to solve micro-assembling problems was the use of micro-machines that can build or assemble other micro-machines consisting of different micro-devices, or called micro-factory [1]. Almost forty years later, research publications on micro-robot appear as application papers in medical technology field. Colonoscopy by using micro-robot for diagnostic cancer in colon was presented [2]. Micro-robot used in ultrasonography in kidney [3] and used in biomedicine [4], [5]. All of them allow advanced computer-assisted surgery and surgery over the Internet. Moreover, flexible active endoscopes can react to instructions simultaneously in order to assist the surgeon and enter to blood vessels and various cavities where they can complicatedly measure and manipulate. Additionally, in the production area, micro-assembly and micro-factory or desktop station fabrication were used to capture sort and combine cells [6]-[8]. A solar micro-robot is researching for space exploration [9]. Micro-robot can use in industrial inspections to inspect plant, investigate an engine, examine circuit board and monitor air pollution or weather [10]. Consequently, micro-robot can meet these demands.

Although there are a variety of micro-robots, that require high power consumption by inductive coupling [11], vibration [12], thermo-electro-mechanical [13] and gold bonding wire [14]-[17] very complex wireless power supply transmission. The performance of micro-robot operation range and the stiffness of wires can degrade the controllability. The problem of friction such as bearings or sliding contacting in their motors can degrade the controllability. Almost all of hybrid micro-robots can cause high cost operation. The capacitively coupled electrostatic power delivery mechanism is presented for untethered micro-robot [18]. However, it has limited movement. The comparison of micro-robots is shown in Table I.

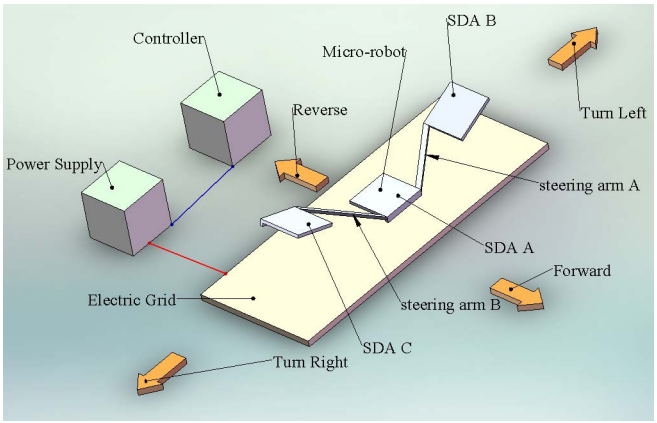

Fig. 1. Micro-robot consists of three scratch drive actuators and two steering arms.

As a step towards the goal of creating wireless micro-robot with a monolithically silicon batch-fabrication process, this paper describes the design and controllability of wireless, walking electrostatic MEMS micro-robot with dimensions of 365 µm x 75 µm. As shown in Fig. 1, it consists of three scratch drive actuators (SDA) and two steering arms. The scratch drive actuators create movement in horizontal direction and the steering arms create movement in vertical direction.

II. MICRO-ROBOT DESIGN AND DESCRIPTION

A. Steering Arm

The micro-robot operates in two actions: propulsion and tilt up or down. In order to control the micro-robot, each actuator has to operate in different voltage separately. The different curved cantilever beams, or steering arms, have different snap-down voltage and release voltage, where snap down voltage is the voltage that deflects beam to contact with the electrodes and release voltage is the voltage that snaps upward beam.

TABLE I. COMPARISON OF MICRO-ROBOT DIMENSIONAL PARAMETER

Micro-robot type	Size	Total mass	Total actuator mass	Energy source
Photothermal transduction [13]	in order of 3 mm	N/A	N/A	Light source
Electric through gold bonding wire of 2 degrees-of-freedom micro-robot leg [15]	1 cm x 1 cm x 0.5 mm	127.5 mg	2.21 x 10^{-3} mg	Voltage source 0-5 V
Electric through gold bonding wire of 1 degrees-of-freedom micro-robot leg [15]	5 mm x 5 mm x 0.5 mm	32 mg	2.00 x 10^{-3} mg	N/A
MINIMAN series [26]	≈ 170 cm^3	N/A	N/A	Voltage source ±150 V
Thermal microactuator array [16]	30 mm x 10mm x 1 mm	0.457 g	N/A	Voltage source 60 V
Polyimide joint actuator [14]	15 mm x 5 mm x 1.5 mm	≈ 100 mg	0.161 mg	Square Voltage of 20 V
Solar power [9]	8.5 mm x 4 mm x 0.5 mm	10.2 mg	6.4 mg	Solar-cell/high-voltage-buffer chip 50 V

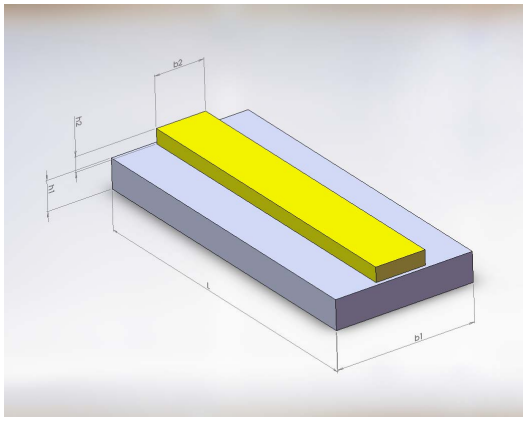

Fig. 2. Schematic of a cantilever beam composed of two thin film stack.

By using residual stress technique, each steering arm can be bent differently [21]-[22]. Because polysilicon layer has a compressive residual stress while the metal layer has highly tensile residual stress in MUMPs technology, as shown in Fig. 2, cantilever beam with long L consists of bottom polysilicon structural layer and upper metal structural layer with residual stress σ_1 and σ_2, Young's modulus E_1 and E_2, width b_1 and b_2, film thickness h_1 and h_2 respectively. After post processing, the released structure will bend upward. Generally, beam deposited with gold layer will curl up about 6 μm per 100 μm in length.

The radius of curvature can be derived as [22]:

$$\frac{1}{\rho} = \frac{6\beta n(1+n)(m\sigma_2 - \sigma_1)}{h_2 E_2[K + 3m^* n(1+n)^2]} \tag{1}$$

and the end displacement (δ) of the beam perpendicular to the pre-release position can be derived as [22]:

$$\delta = \rho\left[1 - \cos\left(\frac{L}{\rho}\right)\right] \tag{2}$$

where $K = 1 + 4m^* n + 6m^* n^2 + 4m^* n^3 + m^{*2} n^4$, $m^* = m \cdot \beta$, $m = E_1 / E_2$, $\beta = b_1 / b_2$, $n = h_1 / h_2$.

From equations (1)-(2), the beam width does not have influence on the beam end displacement. However, the beam width relates to the area of steering arm that impacts snap-down voltage and release voltage.

B. Electrode

In order to move micro-robot without wire, the capacitive coupling with substrate is used [18]-[20]. Electrical power and control signal via electrodes on the substrate are sent to micro-robot. The operating environment that uses capacitive coupling must have constant voltage on the micro-robot in every position on the electric grid. The potential is applied on micro-robot [19]

$$V_{micro-robot} = \frac{V_1 C_1 + V_2 C_2}{C_1 + C_2} \tag{3}$$

where V_1 and V_2 are the applied voltage, and C_1 and C_2 are the capacitance that is proportional to the area of overlap between the micro-robot and the low-voltage and high-voltage electrodes, respectively. Idealistically, the potential induced between micro-robot and any of electrical grids beneath it will be roughly half of that voltage applied between the electrical grids themselves.

C. Snap up and snap down voltage

To control each steering arm, the snap-down and release voltages are considered. When voltage is applied between electrodes and steering arm, that is hanged over electrodes, steering arm bends down because of electrostatic attraction. The electromechanical analysis of cantilever snap-down voltage or pull-in voltage (V_{PI}) and release voltage (V_R), respectively, that are expressed as [18], [23]:

TABLE II. MATERIAL PROPERTEIS OF THIN FILMS USED FOR ANALYTICAL SOLUTIONS AND ANSYS SOLUTIONS

Material Properties	Properties Value
Thickness of plate and steering arm	1.5 μm
Polysilicon Young's Modulus	158 *GPa*
Gold Young's Modulus	78 *GPa*
Polysilicon Residual Stress	-10 *MPa*
Gold Residual Stress	50 *MPa*
Polysilicon Density	2.33 x 10^{-15} kg/ μm^3
Gold Density	1.93 x 10^{-14} kg/ μm^3

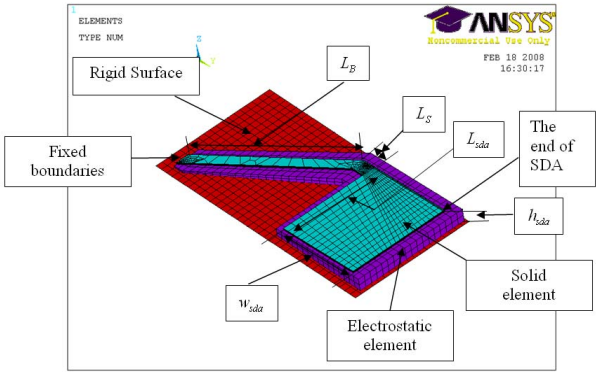

Fig. 3. The Dimension of micro-robot's structure.

$$V_{PI} = \sqrt{\frac{8}{27}\frac{K_0\delta_0^3}{\varepsilon_0 A}} \tag{4}$$

$$V_R = \sqrt{\frac{2K_0\delta_1^2(\delta_0-\delta_1)}{\varepsilon_0 A}} \tag{5}$$

where K_0 is mechanical spring constant, δ_0 and δ_1 are equilibrium spacing when applied zero voltage and snap-down voltage on electrodes respectively, ε_0 is permittivity of air and A is area of cantilever.

III. MICRO-ROBOT SIMULATION RESULT

All simulations were carried out using ANSYS software version 11.0. The mechanical properties of polysilicon and metal layers are listed in Table II presented by MUMPs foundry [24] and [25].

In micro-robot simulation, three dimensional-model is built and micro-robot is modeled by SOLID45 structural solid while air is modeled by SOLID122 tetrahedral electrostatic solid. The surface flags (FSIN) are placed on the bottom of micro-robot structure and the top of electrostatic solid. In order to prepare the movement of electrostatic solid, the morphing command is

TABLE III. DIMENSIONAL PARAMETER

Model	h_{sda} (μm)	L_B (μm)	L_S (μm)	w_{sda} (μm)	L_{sda} (μm)
Micro-robot's left part	8.247	100	10	65	75
Micro-robot's right part	7.423	100	10	65	75

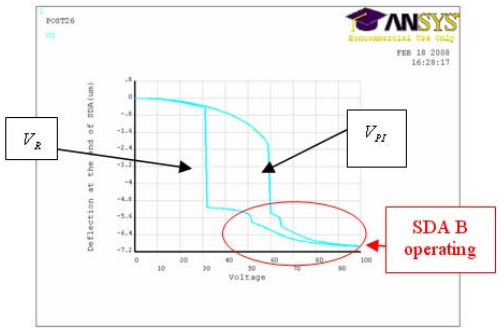

Fig. 4. Hysteresis band shows displacement of the end of SDA for left part of micro-robot when applying voltage 0 to 100 V and back to 0 V.

activated. To prevent the electrostatic attraction and the steering arm and SDA bending beyond the substrate, TARGET170 3-D Target Segment element and CONTA174 3-D 8-Node Surface-to-Surface Contact are used. In this finite element model, CNOF is activated to specify a contact surface offset that equals to 0.6 μm.

Fig. 3 and Table III show the dimension of simulated element SDA B and steering arm A, or left part, of micro-robot's structure, and SDA C and steering arm B, or right part of micro-robot's structure.

In order to control and select condition arbitrarily, it is obligatory that the hysteresis bands of states are nested. The hysteresis band characteristic explains the snap down voltage and snap up voltage. From Fig. 4, the hysteresis band of micro-robot's left part shows the snap down voltage equaling to 60 V and snap up voltage equaling to 31 V. In the same way, the simulation results show the hysteresis band of micro-robot's right part that has snap down and snap up voltage equaling to 42 V and 38 V, respectively. As the results, the hysteresis band of micro-robot's right part is nested in that of micro-robot's left part. Fig. 5 show the deflection when it is biased 100 V.

The operating environment of micro-robot consists of interdigitated polysilcon that is coated with silicon dioxide used as dielectric layer. Each of interdigitated polysilicion is separated with dielectric material. Four types of different shapes, that are rectangle, square wave, hexagonal wave and triangular wave electrical grid model, is investigated. SOLID123 3-D 10-Node Tetrahedral Electrostatic Solid is selected element. Regarding Fig. 6, the triangular wave electrical grid model is applied 100 V and 0 V. The simulation results of electric field vector summation is shown in Fig. 7. The electric field vector summation of triangular wave

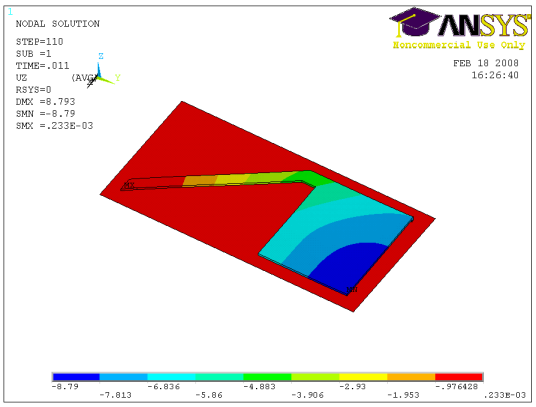

Fig. 5. Deflection for a bias of 100V at the left part of micro-robot.

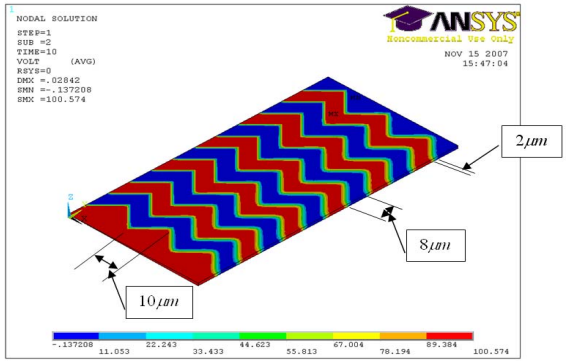

Fig. 6 Triangular wave electrical grid model applied 100 V and 0 V.

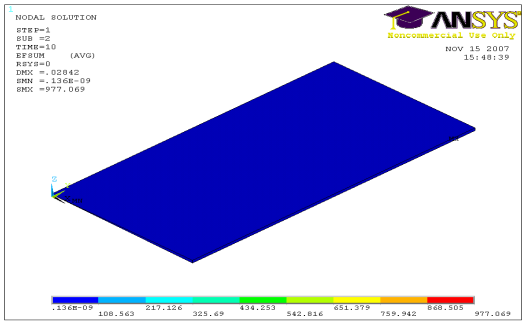

Fig.7 Simulation results of electric field vector summation at triangular wave electrical grid model.

electrical grid model is almost the same in every point on the substrate that meets the requirement of micro-robot environment.

Unlike triangular wave electrical grid model, rectangle, square wave and hexagonal wave electrical grid model have varied a lot of electric field in each point. Then, micro-robot's environment cannot maintain the constant voltage in every position.

TABLE IV. VOLTAGE OPERATION

Voltage	Operation
V10	SDA C Flexure
V9	SDA C Relaxation
V8	Steering Arm B down
V7	SDA B Flexure
V6	SDA B Relaxation
V5	Steering Arm A down
V4	Steering Arm A up
V3	Steering Arm B up
V2	SDA A Flexure
V1	SDA A Relaxation

IV. CONTROL SYSTEM DESIGN

The hysteresis bands of each steering arm must be nested within one another. Consequently, the micro-robot can be controlled status independently as described in Table IV. It shows the voltage level for controlling micro-robot, when V1 < V2 < V3 < V4 < V5 < V6 < V7 < V8 < V9 < V10 make control signals. For instance, when applied V2 and followed by V1, micro-robot moves forward because SDA A flexes and relaxes. When micro-robot is required to move steering arm A down, at the first, voltage V8 is applied. In this state steering arm A and B bend down. Next, electric grid applies V4 in order to bend steering arm A upward but steering arm B is still bend down because voltage is not lower than V3. From voltage operation as shown in Table IV, micro-robot can be completely controlled.

V. CONCLUSION AND FUTURE WORK

In this paper, wireless walking scratch drive MEMS micro-robot design is presented. Micro-robot can be controlled and powered by capacitive coupling. Electromechanical hysteresis stored in the micro-robot's structure is utilized to control each characteristic independently. As the results, micro-robot can move left, right, forward and reverse direction. From the simulation result of electric grid in four models, the electric field vector summation of triangular wave electrical grid model is the most suitable, due to uniform of the electric field in every point.

In future work, accurate mathematical model will be presented and compared with the experimental data. Regarding fully control manner, finite state machine will be used to control the micro-robot. Micro-robot is being fabricated by POLYMUMPs process and deposited dielectric material in the post processing.

ACKNOWLEDGMENT

This work has been funded partially by Sensor Technology Program, National Electronic and Computer Technology Center (NECTEC), Thailand and Royal Thai Government (RTG) granting to AIT.

REFERENCES

[1] R.P. Feynman, “There's plenty of room at the bottom”, Journal of Microelectromechanical Systems, Vol. 1, Issue 1, pp.60-66, Mar. 1992.

[2] P. Dario, M.C. Carrozza, L. Lencioni, B. Magnani and S. D'Attanasio, "A microrobotic system for colonoscopy", IEEE International Conference on Robotics and Automation 1997, vol.2, pp.1567 – 1572, Apr. 1997.

[3] Y. Haga, Y. Tanahashi and M. Esashi, "Small diameter active catheter using shape memory alloy", The Eleventh Micro Electro Mechanical Systems, pp.419 – 424, Jan. 1998.

[4] F. Tendick, S.S. Sastry, R.S. Fearing and M. Cohn, "Applications of micromechatronics in minimally invasive surgery, IEEE/ASME Transactions on Mechatronics, Vol. 3, Issue 1, pp.34 – 42 , March 1998.

[5] Ki-Tae Park and M. Esashi, "A multilink active catheter with polyimide-based integrated CMOS interface circuits", Journal of Microelectromechanical Systems, Vol 8, Issue 4, pp.349 – 357, Dec. 1999.

[6] F. Fatikow and U. Rembold, "An automated microrobot-based desktop station for micro assembly and handling of micro-objects", IEEE Conference on Emerging Technologies and Factory Automation, vol.2, pp.586 – 592, Nov. 1996.

[7] H. Ishihara, T. Fukuda, K. Kosuge, F. Arai and K. Hamagishi, "Approach to distributed micro robotic system. Development of micro line trace robot and autonomous micro robotic system", IEEE Conference on Emerging Technologies and Factory Automation 1995, Vol. 1, pp.375 – 380, May 1995.

[8] J. Ok, Milton Chu and Chang-Jin Kim, "Pneumatically driven microcage for micro-objects in biological liquid", Twelfth IEEE International Conference on Micro Electro Mechanical Systems, pp.459 – 463, Jan. 1999.

[9] Hollar S., Flynn A., Bellew C. and Pister K.S.J., "Solar powered 10 mg silicon robot**",** IEEE The Sixteenth Annual International Conference on Micro Electro Mechanical Systems, pp. 706 – 711, 19-23 Jan. 2003.

[10] M. Takeda, "Applications of MEMS to industrial inspection", The 14th IEEE International Conference on Micro Electro Mechanical Systems, pp.182 – 191, 21-25 Jan 2001.

[11] P. Basset, A. Kaiser, P. Bigotte, D. Collard and L. Buchaillot, "A large stepwise motion electrostatic actuator for a wireless microrobot", IEEE Con. MEMS 15th 2002, pp. 606-609.

[12] K. Suzuki, I. Shimoyama and H. Miura, "Insect-model based microrobot with elastic hinges", Journal of Microelectromechanical Systems, Vol. 3, Issue 1, pp.1-9, Mar 1994.

[13] S. Baglio, S. Castorina, L. Fortuna and N. Savalli, "Development of autonomous, mobile micro-electro-mechanical devices", IEEE International Symposium on Circuits and Systems, vol.4, pp. IV-285 - IV-288, May 2002.

[14] T. Ebefors, J. U. Mattsson, E. Kälvesten, and G. Stemme, "A walking silicon micro-robot," Transducers, Jun. 1999, pp. 1202–1205.

[15] P. E. Kladitis and V. M. Bright, "Prototype microrobots for micro-positioning and micro-unmanned vehicles," Sens. Actuators A, Phys., vol.A80, no. 2, 2000, pp. 132–137.

[16] M. H. Mohebbi, M. L. Terry, K. F. Böhringer, G. T. A. Kovacs, and J. W. Suh, "Omnidirectional walking microrobot realized by thermal microactuator arrays," Proc. ASME. Int. Mechanical Engineering Congress and Exposition, pp. 1–7, Nov. 2001.

[17] R. J. Linderman and V. M. Bright, "Optimized scratch drive actuator for tethered nanometer positioning of chip-sized components," Transducers , pp. 214–217, Jun. 2000.

[18] B.R Donald, C.G. Levey, C.D. McGray, I. Paprotny and D. Rus, "An untethered, electrostatic, globally controllable MEMS micro-robot", Journal of Microelectromechanical Systems, Volume 15, Issue 1, pp. 1 – 15, Feb. 2006.

[19] B.R Donald, C.G. Levey, C.D. McGray, D. Rus and M. Sinclair, "Power Delivery and Locomotion of Untethered Microactuators", J.MEMS, Vol. 12, No.6, pp.947-959, Dec.2003.

[20] L.G. Frechette, S.F. Nagle, R. Ghodssi, S.D. Umans, M.A. Schmidt and J.H. Lang, "An electrostatic induction micromotor supported on gas-lubricated bearings", The 14th IEEE International Conference on Micro Electro Mechanical Systems, pp. 290 – 293, 21-25 Jan.

[21] M.W. Judy, Y.-H. Cho, R.T. Howe and A.P. Pisano, "Self-adjusting microstructures (SAMS)", Proceedings An Investigation of Micro Structures, Sensors, Actuators, Machines and Robots, pp. 51 – 56, Jan .

[22] Xiaohong Mu, M. Kahrizi, and L. Landsberger, "Design & Fabrication of Out-of-Plane Electrostatic Actuators for Optical Application", Canadian Conference on Electrical and Computer Engineering, pp.133-136, 4-7 May, vol.1.

[23] H.C. Nathanson, W.E. Newell, R.A. Wickstrom and J.R. Davis, "The resonant gate transistor", IEEE Trans. Electron Devices, vol.14, pp.117-133, Mar 1978.

[24] David Koester, Allen Cowen, Ramaswamy Mahadevan, Mark Stonefield and Busbee Hardy, PolyMUMPs Design Handbook, a MUMPs process revision 11.0.

[25] Vamsee K. Pamula, Anand Jog, and Richard B. Fair, "Mechanical Property Measurement of thin-film gold using thermally actuated bumetallic cantilever beams" Modeling and Simulation of Microsystems 2001.

[26] H. Worn, F. Schmoeckel, A. Buerkle, J. Samitier, M. Puig-Vidal, S. Johansson, U. Simu, J.-U. Meyer, and M. Biehl, "From decimeter- to centimeter-sized mobile microrobots—The development of the miniman system," Proc. SPIE Microrobotics and Microassembly III, vol. 4568, pp. 175–186, 2001.